Polarised Single-crystal Electronic Absorption Spectra of Tetraphenylarsonium Tetrahalogenonitrido-osmate(VI) Compounds and the Crystal and Molecular Structures of Tetraphenylarsonium Tetrabromonitrido-osmate(VI)

By **David Collison, C. David Garner, Frank E. Mabbs,*** and **John A. Salthouse,** Department of Chemistry, Manchester University, Manchester M13 9PL
Trevor J. King, Department of Chemistry, Nottingham University, Nottingham NG7 2RD

The single-crystal polarised electronic absorption spectra of $[AsPh_4][OsNX_4]$ (X = Cl, Br, or I) at room temperature and 5 K are reported in the range 10 000—40 000 cm^{-1}. The spectra have been interpreted using the observed polarisation and vibrational fine-structure data in conjunction with a parameterised ligand-field model. The single-crystal structure of $[AsPh_4][OsNBr_4]$ has been determined by *X*-ray crystallography. The compound crystallises in the tetragonal space group $P4/n$, $a = b = 12.774(3)$, $c = 8.008(3)$ Å, $Z = 2$. The $[OsNBr_4]^-$ ion has $4mm$ (C_{4v}) symmetry with Os–N 1.583(15), Os–Br 2.457(1) Å, N–Os–Br 104.29(3)°. The $[AsPh_4]^+$ cation has crystallographic $\bar{4}$ (S_4) symmetry with As–C 1.891(8) Å, C–As–C 105.12(48) and 116.69(25)°.

ALTHOUGH compounds containing the MN^{n+} chromophore, where M = Ru or Os, have been known for a number of years there is a dearth of absorption spectral data compared with the MO^{n+} species of the early transition-metal elements. Polarised single-crystal electronic absorption spectra have been reported for $K[OsO_3N]$ doped in $K[ClO_4]$,[1] whilst the thin-film technique of Cowman *et al.*[2] has been used to study $[OsNX_4]^-$ and $[OsNX_4(OH_2)]^-$ chromophores, where X = Cl or Br. However, this latter technique appears to have serious limitations since only the *xy* polarised spectrum was observed directly, the *z* polarised spectrum being obtained by subtracting the *xy* from that of a mull. In view of this lack of data on the above types of chromophores, we now report the low-temperature polarised single-crystal electronic absorption spectra of the compounds $[AsPh_4][OsNX_4]$ (where X = Cl, Br, or I). Also, we have determined the crystal structure of $[AsPh_4][OsNBr_4]$ which, like other salts of this series, crystallises in the tetragonal space group $P4/n$[3,4] and contains discrete square-pyramidal $[MNX_4]^-$ anions having C_{4v} point symmetry, with all the M–N vectors parallel to each other and to the crystallographic *c* axis.

EXPERIMENTAL

Preparation of the Compounds.—$[AsPh_4][OsNX_4]$ [X = Cl or Br) were prepared by the method of Griffith and Pawson.[5] Crystals of the chloride were grown by slow evaporation of a solution of the compound in CH_2Cl_2, whilst MeCN solvent was used to crystallise the bromo-complex.

$[AsPh_4][OsNI_4]$ was prepared by refluxing $[AsPh_4][OsNCl_4]$ in MeI–MeCN (10 : 1 by volume) for 3 h. Removal of the solvent under reduced pressure gave a deep red powder which was recrystallised from MeI–MeCN (1 : 1 by volume).

The crystallisations of all three compounds were performed in the dark. Elemental analyses on the compounds were in agreement with their formulations. Also i.r. spectra for the above compounds were in agreement with published data,[6] which are summarised in Table 1.

Electronic Absorption Spectra.—These were measured in the range 10 000—40 000 cm^{-1} on suitably thinned crystals mounted on silica plates at room temperature and at 5 K using equipment previously described.[7] The orientations of the crystals were such that the electric vector of the incident beam could be polarised parallel to and perpendicular to the crystallographic *c* axis. The data obtained at 5 K are given in Tables 2—4 and in Figure 1—3, which also include the room-temperature spectra.

TABLE 1

Vibrational frequencies (cm^{-1}) * for $[MNX_4]^-$ (M = Ru or Os, X = Cl or Br)

Mode	$[OsNCl_4]^-$	$[OsNBr_4]^-$	$[RuNCl_4]^-$	$[RuNBr_4]^-$
ν_1, A_1 ν(MN)	*1 123vs*	*1 119vs*	*1 092vs*	*1 088vs*
ν_2, A_1 ν(MX)	358 (10)	162 (4)	346 (10)	224 (10)
ν_3, A_1 π(MX)	184 (6)	122 (5)	197 (8)	156 (1)
ν_4, B_1 ν(MX)	352 (1)	156 (1)	304 (4)	187 (3)
ν_5, B_1 π(MX)	149 (1)	110 (1)	154 (1)	103 (1)
ν_6, B_2 δ(MX)	174 (2)	120 (2)	172 (5)	128 (1)
ν_7, E ν(MX)	*365vs*	*220m*	*378vs*	*304vs*
ν_8, E δ(NMX)	*271m*	*273m*	*267s*	211
ν_9, E δ(XMX)	132 ($\frac{1}{2}$)	98 (1)	163 (1)	98

* Infra-red frequencies (ref. 6) are given in italics; *vs* = Very strong, *s* = strong, *m* = medium. Raman frequencies (ref. 8) have relative intensities in parentheses. In all cases the cation was $[AsPh_4]^+$.

Single-crystal Structure.—*Crystal data.* $C_{24}H_{20}AsBr_4NOs$, $M = 907.1$, Tetragonal, $a = b = 12.774(3)$, $c = 8.008(3)$ Å, $U = 1\,306.7$ Å^3, D_m (flotation) = 2.28, $Z = 2$, D_c = 2.30 g cm^{-3}, $F(000) = 840$, Mo-K_α radiation, $\lambda = 0.7107$ Å, μ(Mo-K_α) = 130 cm^{-1}. Space group $P4/n$ from systematic absences: $hk0$ when $h + k \neq 2n$.

Preliminary unit-cell dimensions and space-group data were obtained from oscillation and Weissenberg photographs and refined on a Hilger and Watts four-circle diffractometer. The layers 0—12*kl* were examined for a needle-shaped crystal *ca.* 4 mm in length and 0.2 mm in cross-section and 1 299 reflections with $I > 3\sigma(I)$ in the range $0 < 2\theta < 55°$ were considered and used in the subsequent refinement. No corrections were made for absorption, anomalous dispersion, or secondary extinction. Data reduction and crystallographic calculations were carried out on the Nottingham I.C.L. 1906A computer using the Oxford University CRYSTALS programs. Atomic scattering factors were used as published.[8] The structure was solved by

TABLE 2

Band positions (cm^{-1}) for the polarised single-crystal electronic absorption spectrum of $[AsPh_4][OsNCl_4]$ at 5 K *

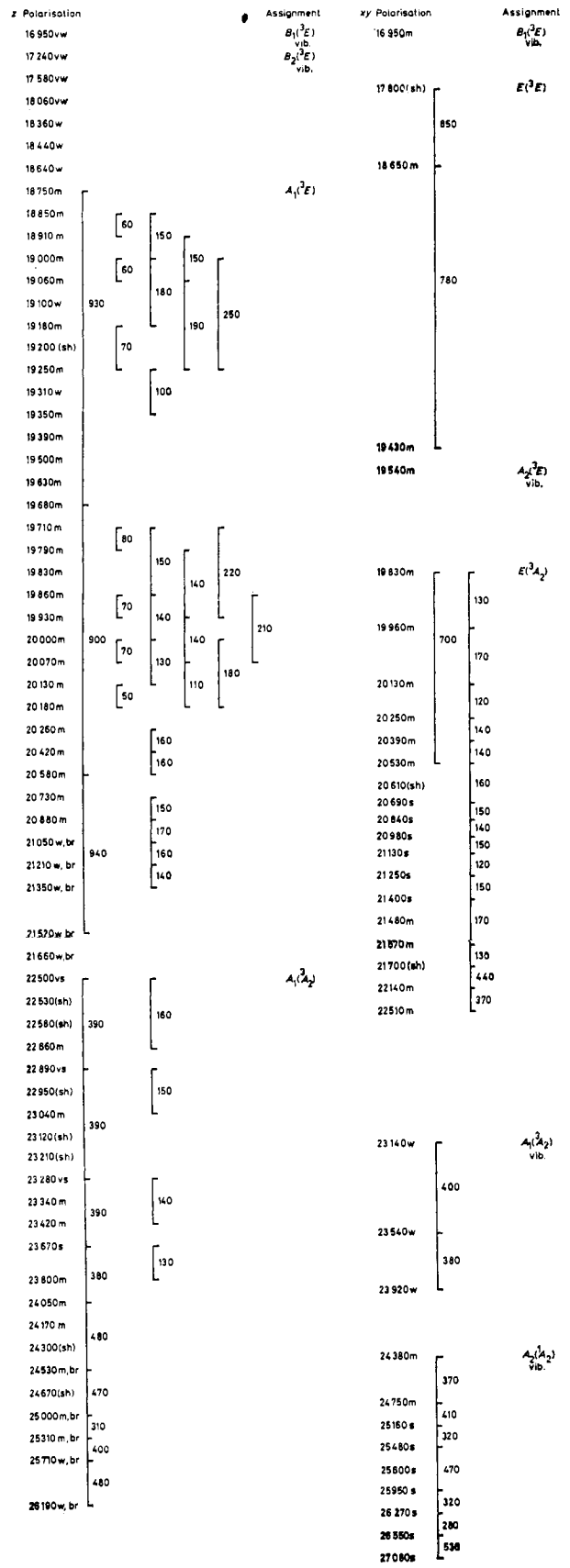

TABLE 2 (*continued*)

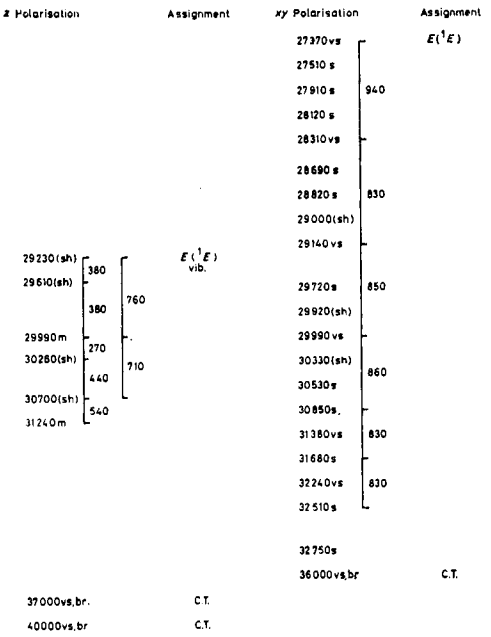

* Assignment refers to the electronic excited-state label of the electronic transition from the $A_1(^1A_1)$ ground state; 'vib.' denotes that the transition is vibronically allowed; C.T. = charge transfer; s = strong, m = medium, w = weak, (sh) = shoulder, br = broad, v = very.

TABLE 3

Band positions (cm^{-1}) for the polarised single-crystal electronic absorption spectrum of $[AsPh_4][OsNBr_4]$ at 5 K *

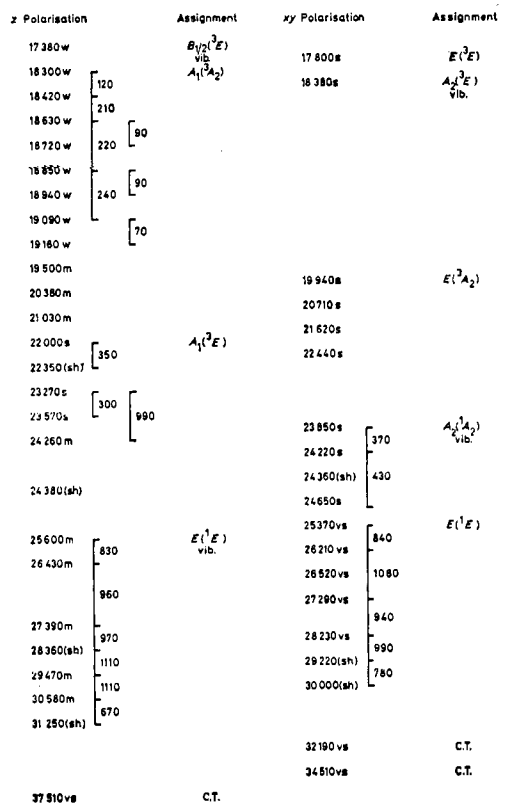

* See footnote to Table 2.

normal heavy-atom, Patterson, and Fourier techniques and refined by least-squares procedures involving anisotropic temperature factors for all the non-hydrogen atoms. The hydrogen atoms were included in the refinement at fixed positions and each with a constant U_{iso}. The analysis converged at R 0.041. Structure factors and thermal parameters are in Supplementary Publication No. SUP 23086 (15 pp.).*

TABLE 4

Band positions (cm^{-1}) for the polarised single-crystal electronic absorption spectrum of $[AsPh_4][OsNI_4]$ at 5 K *

z Polarisation	Assignment	xy Polarisation	Assignment
17 700w		17 710s	$E(^3E)$
18 490(sh)	$A_1(^3A_2)$	18 620(sh)	
18 950(sh)		19 620s	$E(^3A_2)$
19 770m		20 700(sh)	
21 340s	$A_1(^3E)$	21 250s	
22 310s		22 210s	$A_2(^1A_2)$ vib.
22 670(sh)		22 940s	$E(^1E)$
23 910m		24 010s	
24 850m		24 480s	
26 060m		25 020s	
		26 000(sh)	
		27 130(sh)	

* See footnote to Table 2.

RESULTS AND DISCUSSION

Crystal Structure.—The final atomic co-ordinates are listed in Table 5 and selected bond lengths and angles are in Table 6. The Os–N bond length [1.583(15) Å] and the interligand bond angles in the $[OsNBr_4]^-$ ion are in good agreement with those reported for the isomorphous chloro- and iodo-complexes.[3,4] The dimensions within the $[AsPh_4]^+$ ion are also in agreement with the corresponding dimensions reported for this cation in the chloro- and iodo-compounds.

TABLE 5

Atomic co-ordinates for $[AsPh_4][OsNBr_4]$ with estimated standard deviations in parentheses

	x/a	y/b	z/c
Os(1)	0.250 00	0.250 00	0.120 09(8)
N(1)	0.250 00	0.250 00	−0.077 63(184)
Br(1)	0.091 49(8)	0.348 05(9)	0.195 84(14)
As(1)	0.250 00	0.750 00	0.000 00
C(1)	−0.258 59(62)	0.132 78(60)	0.143 56(99)
C(2)	−0.190 63(80)	0.127 80(70)	0.282 45(102)
C(3)	−0.202 28(88)	0.047 74(84)	0.396 96(130)
C(4)	−0.274 96(100)	−0.025 70(87)	0.371 23(141)
C(5)	−0.341 41(83)	−0.024 21(77)	0.236 98(143)
C(6)	−0.332 14(69)	0.054 93(63)	0.116 95(125)
H(2)	−0.137 21	0.184 00	0.304 61
H(3)	−0.153 34	0.045 96	0.501 11
H(4)	−0.278 30	−0.085 24	0.460 69
H(5)	−0.397 07	−0.079 34	0.238 53
H(6)	−0.376 96	0.054 35	0.011 94

Electronic Absorption Spectra.—Since the single-crystal polarised spectra at room temperature showed very poor resolution, the results are merely summarised in the Figures. However, cooling the crystals to 5 K afforded considerable resolution, particularly for the chloro-complex, and since we base our assignments on these spectra they are reported in detail. Our approach to the interpretation of the spectra is to select $[AsPh_4][OsNCl_4]$, which gave the most detailed information, and to assign as many bands as possible based on the polarisation data. This is then followed by a discussion of the vibrational fine structure, supplemented by a ligand-field calculation (see Appendix for details).

TABLE 6

Bond lengths (Å) and interbond angles (°) for $[AsPh_4][OsNBr_4]$

(*a*) Co-ordination about Os

Os(1)–N(1)	1.583(15)	N(1)–Os(1)–Br(1)	104.29(3)
Os(1)–Br(1)	2.457(1)	Br(1)–Os(1)–Br(1)′	151.41(6)
		Br(1)–Os(1)–Br(1)″	86.51(1)

(*b*) In the $[AsPh_4]^+$ cation

As(1)–C(1)	1.891(8)	C(1)–As(1)–C(1)′	105.12(48)
C(1)–C(2)	1.412(12)	C(1)′–As(1)–C(1)″	111.69(25)
C(1)–C(6)	1.385(12)	As(1)–C(1)–C(2)	118.61(60)
C(2)–C(3)	1.382(13)	As(1)–C(1)–C(6)	120.97(68)
C(3)–C(4)	1.336(17)	C(2)–C(1)–C(6)	120.39(77)
C(4)–C(5)	1.370(16)	C(1)–C(2)–C(3)	119.33(89)
C(5)–C(6)	1.400(13)	C(2)–C(3)–C(4)	119.49(99)
		C(3)–C(4)–C(5)	122.81(97)
		C(4)–C(5)–C(6)	119.77(98)
		C(5)–C(6)–C(1)	118.06(93)

The electronic ground states of the complexes comprise a pair of electrons in a metal-based d_{xy}* antibonding molecular orbital which leads to a $^1A_1$ ground term consistent with their diamagnetism.[9] Single electron excitations from this ground state to the other metal-based antibonding molecular orbitals give rise to a number of spin-triplet and spin-singlet excited states, see Table 7. In the absence of spin–orbit coupling, the selection rules for electric-dipole transitions predict only one allowed band which should occur in xy polarisation. Clearly our spectra are more complex than this. It is expected that spin–orbit coupling would be a significant perturbation for Os^{6+} and, as shown in Table 7, this may

TABLE 7

Selection rules [a] for electric dipole transitions of a d^2 complex

	C_{4v} polarisation			C_{4v}' polarisation	
Transition [b]	z	xy	Transition [c]	z	xy
$(xy)b_2 \rightarrow a_1(z^2)$					
$^1A_1 \rightarrow {}^3B_2$	F	F	$A_1 \rightarrow B_1$	F(B_1)	F(E)
			$\rightarrow E$	F(E)	A
$\rightarrow {}^1B_2$	F(B_2)	F(E)	$\rightarrow B_2$	F(B_2)	F(E)
$(xy)b_2 \rightarrow b_1(x^2-y^2)$					
$\rightarrow {}^3A_2$	F	F	$\rightarrow A_1$	A	F(E)
			$\rightarrow E$	F(E)	A
$\rightarrow {}^1A_2$	F(A_2)	F(E)	$\rightarrow A_2$	F(A_2)	F(E)
$(xy)b_2 \rightarrow e(xz,yz)$					
$\rightarrow {}^3E$	F	F	$\rightarrow A_1$	A	F(E)
			$\rightarrow A_2$	F(A_2)	F(E)
			$\rightarrow B_1$	F(B_1)	F(E)
			$\rightarrow B_2$	F(B_2)	F(E)
			$\rightarrow E$	F(E)	A
$\rightarrow {}^1E$	F(E)	A	$\rightarrow E$	F(E)	A

[a] F = Forbidden, A = allowed; the symmetry of the vibration which will make an electronically forbidden band allowed is given in parentheses. Spin selection rule, singlet→triplet, F; singlet→singlet, A. [b] Ground state is $^1A_1$. [c] Ground state is A_1.

* For details see Notices to Authors No. 7, *J. Chem. Soc., Dalton Trans.*, 1980, Index issue.

lead to considerable relaxation of the selection rules. Thus we predict *four* allowed transitions in *xy* polarisation and *two* in *z* polarisation. The ligand-field calculation suggests the following ordering of the excited states involved in these transitions: $E(^3E) < A_1(^3E) < E(^3A_2) < A_1(^3A_2) < A_2(^1A_2) < E(^1E)$. The spectra will now be discussed separately for each compound.

(1) $[AsPh_4][OsNCl_4]$. An examination of the whole spectrum showed three distinct regions of absorption with associated fine structure in *z* polarisation. In *xy* polarisation, structured absorptions were apparent throughout the spectral range. However, a careful analysis of repeating patterns in the fine structure enabled four band systems to be identified which have no counterparts in *z* polarisation. The electronic origins in both polarisations are indicated in Figure 1(*b*) and Table 2.

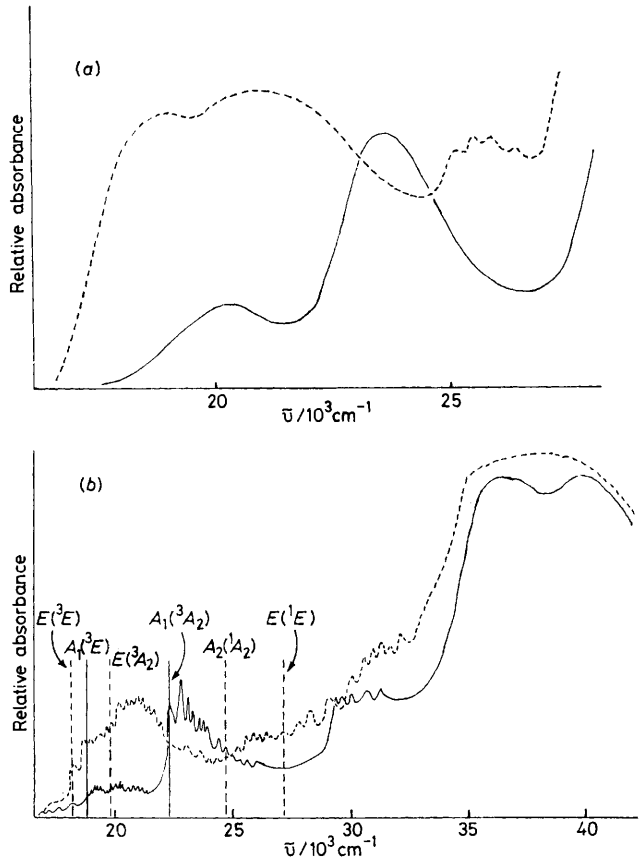

FIGURE 1 Polarised single-crystal electronic absorption spectrum of $[AsPh_4][OsNCl_4]$ at (*a*) 298 K, (*b*) 5 K; *z* polarisation (——), *xy* polarisation (– – – –)

Based on these polarisation data we have assigned the two lowest energy bands in *z* polarisation, originating at 18 750 and 22 500 cm^{-1}, to transitions from the $A_1(^1A_1)$ ground state to $A_1(^3E)$ and $A_1(^3A_2)$ states, respectively. Similarly, bands originating at 17 800, 19 830, and 27 370 cm^{-1} in *xy* polarisation were assigned to transitions to the $E(^3E)$, $E(^3A_2)$, and $E(^1E)$ excited states from $A^1(^1A_1)$, respectively. Additional support for these assignments was obtained from the fine structure associated with each band. This will now be discussed for each individual transition.

$A_1(^1A_1) \rightarrow A_1(^3E)$. A three-membered progression with an average separation between the members of *ca.* 900 cm^{-1} can be identified within this band system. The separations correspond to a ν(Os–N) stretching vibration in the excited state which is reduced from the ground-state value of 1 123 cm^{-1}. The reduction in frequency can be attributed to promotion of an electron into an π^*(Os–N) antibonding molecular orbital. This is consistent with the proposed one-electron promotion $(5d_{xy}^*)^2 \longrightarrow (5d_{xy}^*)^1(5d_{xz}^*, 5d_{yz}^*)^1$. In addition to the vibrational progression involving separations of *ca.* 900 cm^{-1}, there are vibrational progressions involving separations of *ca.* 150 cm^{-1} throughout this band system. Each of these components has a further feature *ca.* 60 cm^{-1} to higher energy. We attribute the separations of *ca.* 150 cm^{-1} to the excited-state A_1 π(OsCl) deformation vibration, reduced from the value of 184 cm^{-1} in the ground state, whilst the separation of *ca.* 60 cm^{-1} is attributed to a lattice vibrational mode.

$A_1(^1A_1) \rightarrow A_1(^3A_2)$. This band system originated at 22 500 cm^{-1} and had a well defined ten-membered vibrational progression with an average spacing of *ca.* 390 cm^{-1}. The first few members of this progression each had an additional splitting of *ca.* 150 cm^{-1} superimposed on them. There were no vibrational features which could be assigned to coupling with an A_1 ν(Os–N) stretching vibration. These observations are consistent with the assignment of the band to a transition involving $A_1(^3A_2)$ which results from the one-electron promotion $(5d_{xy}^*)^2 \longrightarrow (5d_{xy}^*)^1(5d_{x^2-y^2}^*)^1$. The splittings of 390 and 150 cm^{-1} are assumed to correspond to ν_2 [A_1 ν(MX)] and ν_3 [A_1 π(MX)] vibrational modes in the excited state. These splittings agree well with those reported by Cowman *et al.*[2] who identified this band system in their studies. The value of 390 cm^{-1} for ν_2 in the excited state is higher than that observed in the ground state (358 cm^{-1}) and was taken by Cowman *et al.* to be confirmation of the assignment without further comment. Similarly, increases in certain excited-state vibrational frequencies associated with the transition $A_{1g}(^3T_{1g}) \rightarrow T_{1g}(^3T_{1g})$ of $[OsF_6]^{2-}$ have also been reported without further comment.[10] This latter transition arises from the one-electron promotion $(t_{2g})^4 \rightarrow (t_{2g})^3(e_g)^1$, thus corresponding to the promotion of an electron from a π antibonding molecular orbital into an empty σ antibonding molecular orbital. In the present system a simple view of the increase in frequency implies that the promotion of a single electron from a filled metal–chlorine π antibonding molecular orbital to an empty metal–chlorine σ antibonding molecular orbital strengthens the net metal–chlorine interaction! However, such an explanation is chemically not sensible. In our view the most probable explanation for the increase in frequency arises from mixing of the A_1 ν(MX) and A_1 ν(MN) vibrations brought about by spin–orbit coupling admixing the $A_1(^3A_2)$ and $A_1(^3E)$ terms. Since in the excited states the frequency of the A_1 ν(MN) vibration is much greater than that of the

A_1 ν(MX) vibration, it is quite feasible for the net vibrational frequency to be greater than the corresponding frequency in the ground state.

$A_1(^1A_1) \rightarrow E(^3E)$. This transition, originating at 17 800 cm^{-1} in *xy* polarisation, was defined by a three-membered progression with separations of *ca.* 800 cm^{-1} on a rising background of absorption. The assignment of this vibrational structure to the A_1 ν(Os–N) stretching vibration in the excited state, reduced from that in the ground state, is consistent with the promotion of an electron into an π*(Os–N) antibonding molecular orbital. The fine structure coupled with the polarisation of the band is consistent with the excited state arising from the one-electron promotion $(5d_{xy}^*)^2 \longrightarrow (5d_{xy}^*)^1(5d_{xz}^*, 5d_{yz}^*)^1$.

$A_1(^1A_1) \rightarrow E(^3A_2)$. This transition had a band origin at 19 830 cm^{-1} in *xy* polarisation and was associated with vibrational fine structure with an average separation of *ca.* 140 cm^{-1}. There were no separations of *ca.* 390 cm^{-1} as observed for the transition to $A_1(^3A_2)$ in *z* polarisation, nor were there any splittings which were attributable to an A_1 ν(Os–N) stretching vibration. The vibrational progression involving separations of *ca.* 140 cm^{-1} may be attributed to coupling with an A_1 ν(Os–Cl) deformation frequency, reduced from its ground state value of 184 cm^{-1}. The polarisation and vibrational data are consistent with the excited state arising from the one-electron promotion $(5d_{xy}^*)^2 \longrightarrow (5d_{xy}^*)^1(5d_{x^2-y^2}^*)^1$.

$A_1(^1A_1) \rightarrow E(^1E)$. The band attributed to this transition was *xy*-polarised and had its origin at 27 370 cm^{-1}. There was a vibrational progression with average spacing of *ca.* 800 cm^{-1} which we attributed to coupling with the A_1 ν(Os–N) stretching vibration in the excited state. The reduction in the frequency of this mode compared to that in the ground state, and the polarisation, are consistent with the excited state arising from the one-electron promotion $(5d_{xy}^*)^2 \longrightarrow (5d_{xy}^*)^1(5d_{xz}^*, 5d_{yz}^*)^1$.

$A^1(^1A_1) \rightarrow A_2(^1A_2)$. A ligand-field calculation placed $A_2(^1A_2)$ between $A_1(^3A_2)$ and $E(^1E)$ in energy. In addition to this, the selection rules show that this transition is forbidden in *z* polarisation, since these C_{4v} anions have no vibrations of A_2 symmetry, but it can be allowed in *xy* polarisation by coupling with a vibrational mode of *E* symmetry. A band system with its first member at 24 380 cm^{-1}, with an average vibrational splitting of *ca.* 375 cm^{-1} and occurring only in *xy* polarisation, is consistent with these considerations. The vibrational progression is assigned to coupling with an excited-state A_1 ν(Os–Cl) stretching vibration. In the ground state, this vibration has a frequency of 358 cm^{-1}. Again we have an absorption band derived from the one-electron promotion $(5d_{xy}^*)^2 \longrightarrow (5d_{xy}^*)^1(5d_{x^2-y^2}^*)^1$ in which there is an increase in the ν_2 vibrational frequency in the excited state compared to that in the ground state. We propose that the explanation for this increase is the same as that mentioned previously, *i.e.* due to spin–orbit mixing between $A_2(^1A_2)$ and $A_2(^3E)$.

Having assigned most of the stronger features in the spectrum, using primarily the polarisation and fine-structure data, there remained a number of weak features to be accounted for. The approach to their assignment was to rely on the parameterised ligand-field calculation. Initially, a range of ligand-field parameters at the ratios $F_2/F_4 = 21$, 14, and 11, which calculated the energies of the already assigned bands to within *ca.* 500 cm^{-1}, was investigated. Using these parameters as a basis, a best fit set was determined using an iterative least-squares method. In this, all the ligand-field parameters were allowed to vary in predetermined steps away from the starting values until a minimum δ value was found. The term δ is defined as below where *n* is the number of experimentally assigned

$$\delta = 100 \cdot \left(\sum_{i=1}^{n} \Delta E_i^2\right)^{\frac{1}{2}} \Big/ \left[\left\{\sum_{i=1}^{n} (E_i^{\text{obs}})^2\right\} \Big/ n\right]^{\frac{1}{2}}$$

transitions and $\Delta E_i^2 = (E_i^{\text{obs.}} - E_i^{\text{calc.}})^2$. This procedure simultaneously gave the energies of the formally forbidden transitions, and a comparison of the best calculated and observed band positions is given in Tables 2 and 8. In the above calculations a fixed value of $D_3 = 50 \times 10^3$ cm^{-1} was used. This represents the value of D_3 which places transitions involving the electron promotion $(5d_{xy}^*)^2 \longrightarrow (5d_{xy}^*)^1(5d_{z^2}^*)^1$ under the lowest charge-transfer band at *ca.* 36×10^3 cm^{-1}. It is necessary to estimate the energies of such excited states because the *E*, B_1, and B_2 spin–orbit levels of this configuration will interact with levels of the same symmetry which derive from other configurations. The procedure adopted above will *maximise* such interactions.

(2) $[AsPh_4][OsNBr_4]$. The polarised single-crystal electronic absorption spectrum at 5 K (see Figure 2 and Table 3) showed poorer detail compared to that achieved for the corresponding chloro-complex. This may be attributed, at least in part, to lower frequencies for those vibrations involving displacement of the halogen atoms. The major features in the spectrum were assigned in a manner analogous to that used for $[OsNCl_4]^-$. In *z* polarisation, band origins were defined at 17 380 and 22 000 cm^{-1} for the two transitions to the A_1 excited states. The ligand-field calculation indicated that the orbital parentage of these A_1 states is now $A_1(^3A_2) < A_1(^3E)$, the reverse of that for $[OsNCl_4]^-$. This is compatible with the observed vibrational fine structure associated with the appropriate transitions. The band originating at 17 380 cm^{-1} has no fine structure attributable to coupling with an excited-state A_1 ν(Os–N) stretching vibration but does have fine structure with average spacings of 220 cm^{-1}. This fine structure suggests coupling with an excited-state A_1 π(Os–Br) vibration which is increased from the ground-state value of 162 cm^{-1}. A similar increase in frequency was also observed for the band assigned to the transition $A_1(^1A_1) \rightarrow A_1(^3A_2)$ for $[OsNCl_4]^-$. On the other hand, the band originating at 22 000 cm^{-1} has a vibrational progression of average spacing 1 000 cm^{-1} which is attributed to coupling with an A_1 ν(Os–N) stretching vibration in the excited state. This is consistent with the assignment of the transition to the $A_1(^3E)$ excited state arising

TABLE 8

Best-fit ligand-field parameters for $[AsPh_4][OsNX_4]$

Excited states and ligand-field parameters	Band energies */10^3 cm^{-1}					
	X = Cl		X = Br		X = I	
	Obs.	Calc.	Obs.	Calc.	Obs.	Calc.
$B_1(^3E)$	16.95	16.86	17.38	17.21		17.44
$B_2(^3E)$	17.24	17.08	17.38	17.31		17.47
$E(^3E)$	*17.80*	17.68	*17.80*	17.78	*17.71*	17.90
$A_1(^3E)$	*18.75*	18.59	*22.00*	22.00	*21.34*	21.23
$A_2(^3E)$	19.54	19.27	18.38	19.31	18.62	18.79
$E(^3A_2)$	*19.83*	20.35	*19.94*	19.83	*19.62*	19.49
$A_1(^3A_2)$	*22.50*	22.24	*18.30*	18.42	18.49	18.43
$A_2(^1A_2)$	*24.38*	24.11	*23.85*	23.78	22.21	22.01
$E(^1E)$	*27.37*	27.36	*25.37*	25.41	*22.94*	22.99
$B_1(^3B_2)$		35.83		40.70		44.10
$E(^3B_2)$		36.10		40.78		44.12
$B_1(^1B_2)$		45.69		47.31		48.29
$D_1/10^3$ cm^{-1}		31.0		27.4		23.8
$D_2/10^3$ cm^{-1}		24.2		23.9		21.5
$D_3/10^3$ cm^{-1}		50.0		50.0		50.0
F_2/cm^{-1}		1 107.0		680.0		456.0
F_4/cm^{-1}		41.0		42.5		19.0
ξ_{Os}/cm^{-1}		2 800.0		2 700.0		2 100.0
F_2/F_4		27.0		16.0		24.0
δ(%)		2.9		0.7		1.2
Os–X/Å		2.310		2.457		2.662

* Band positions in italics were those assigned and used in the ligand-field fitting procedure.

from the electron promotion $(5d_{xy}^*)^2 \longrightarrow (5d_{xy}^*)^1(5d_{xz}^*,5d_{yz}^*)^1$.

In *xy* polarisation the features originating at 17 800, 23 850, and 25 370 cm^{-1} were assigned to transitions to the excited states $E(^3E)$, $A_2(^1A_2)$, and $E(^1E)$, respectively. The band at 17 800 cm^{-1} showed no vibrational fine structure and the assignment was based on the polarisation data and the results of the ligand-field calculation. The band system starting with the sharp feature at 25 370 cm^{-1} has a somewhat uneven progression of average spacing *ca.* 930 cm^{-1} superimposed on a rising background. These large splittings may be attributed to coupling with an excited-state A_1 ν(Os–N) vibration, and this together with the polarisation of the band is consistent with the assignment of a transition to the $E(^1E)$ excited state resulting from the one-electron promotion $(5d_{xy}^*)^2 \longrightarrow (5d_{xy}^*)^1(5d_{xz}^*,5d_{yz}^*)^1$. The band system starting at 23 850 cm^{-1} was assigned to the transition to the $A_2(^1A_2)$ excited state based on its polarisation properties and on the results of the ligand-field calculations. Although there appeared to be a vibrational progression associated with this band system the details were not readily explicable in terms of the expected coupling with an Os–Br vibration in the excited state.

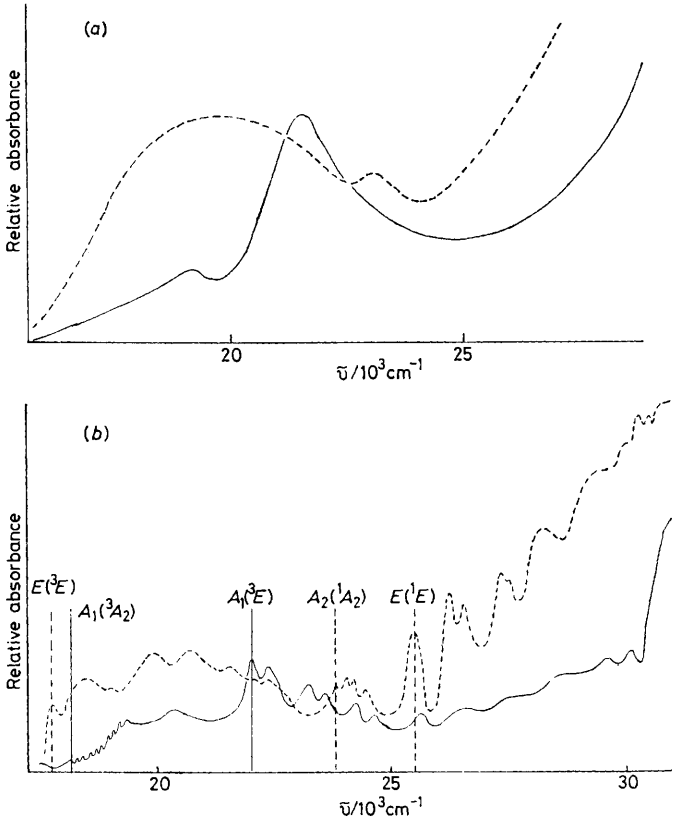

FIGURE 2 Polarised single-crystal electronic absorption spectrum of $[AsPh_4][OsNBr_4]$ at (*a*) 298 K, (*b*) 5 K; *z* polarisation (——), *xy* polarisation (– – – –)

The ligand-field calculation was next used to calculate the energies of the allowed transitions assigned above, and thus to determine the energies of the vibronically allowed transitions. The parameters derived from the least-squares fitting process are given in Table 8.

(3) $[AsPh_4][OsNI_4]$. The polarised electronic absorption spectrum for this compound at 5 K is summarised in Table 4 and Figure 3. The spectrum was not as well resolved and not as clearly polarised as that for the bromo-analogue. Although there appeared to be vibrational fine structure in the spectrum, it was not possible to interpret this as comprehensively as for the two other analogues. The assignment of the spectrum was based on selecting three prominent features in the *xy*-polarised spectrum which have no counterparts in the *z*-

polarised spectrum, and similarly two prominent features in the z-polarised spectrum which have no counterparts in the xy-polarised spectrum. The proposed assignment is indicated in Table 4 and Figure 3 and the best-fit parameters in Table 8. Other assignments of the spectra were tried, but these resulted in significantly higher δ values.

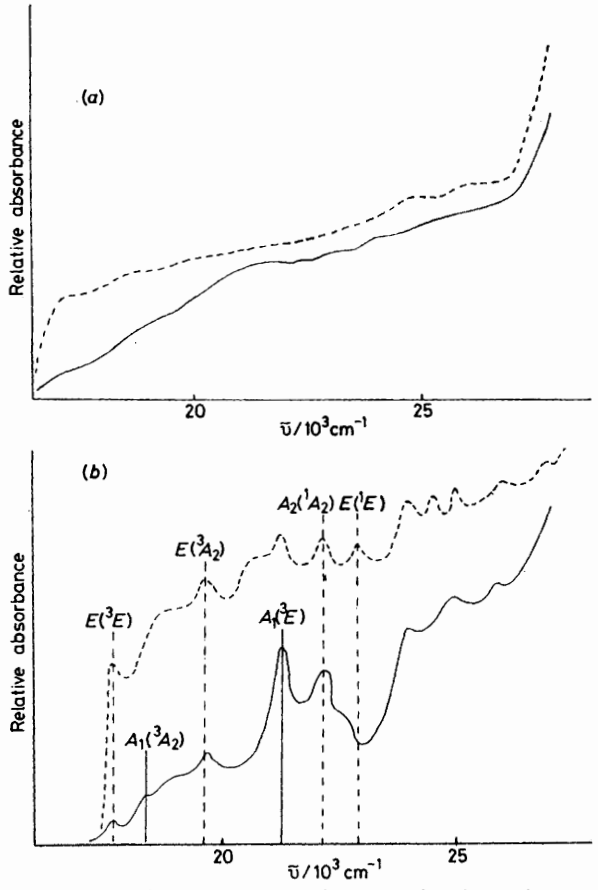

FIGURE 3 Polarised single-crystal electronic absorption spectrum of $[AsPh_4][OsNI_4]$ at (*a*) 298 K, (*b*) 5 K; z polarisation (——), xy polarisation (– – – –)

Ligand-field Parameters.—The values of D_1 and D_2, the splittings between the d_{xy}* and $d_{xz,\,yz}$* and $d_{x^2-y^2}$* orbitals respectively, decrease in the series Cl^-, Br^-, I^-. The trend in D_2 correlates with the expected relative positions of these ligands in the spectrochemical series.[11] However, the d* orbital energies, and hence their mutual separations, depend upon the extent of the covalent bonding within the complex ion. If we assume that the nitrido–metal covalent interaction is dominant, and essentially constant within this series of complexes, then the observed d* orbital splittings are consistent with an increase in covalency of the in-plane ligands on going from chloride to iodide. Furthermore, the decrease in both D_1 and D_2 indicates that the in-plane π bonding increases relatively more rapidly than the in-plane σ bonding as the ligands are changed. This observation correlates with the increasing polarisability of the halide ligands.

The changes in the magnitudes of the metal inter-electronic repulsion parameters, F_k, which should occur when only the in-plane ligands are changed, are difficult to predict. Theoretically it would be expected that decreasing charge, $Z_{\text{eff.}}$, on the metal should decrease F_k, whilst increasing bond length should increase F_k. However, for either of these effects the rate of variation of F_k depends on k. Also the rates of variation of any given F_k will depend on each of these interactions in a different manner. Such a conflict between the theoretical predictions is illustrated by the data for the $Cr^{III}X_6$ (where X = F^-, Cl^-, or Br^-) moieties,[12] where changing X from F^- to Br^- should decrease $Z_{\text{eff.}}$ for chromium whilst the bond lengths increase. For this series, F_2 shows a steady decrease from F^- to Br^- whilst F_4 increases. In the present $[OsNX_4]^-$ systems we find a similar decrease in F_2 when X changes from Cl^- to I^-. However, F_4 shows a slight increase in going from chloride to bromide but a marked decrease for X = I^-. It would appear that on changing from chloride to bromide the effect on F_4 of increasing bond length outweighs the effect of decreasing $Z_{\text{eff.}}$, but in changing to iodide the effect of decreasing $Z_{\text{eff.}}$ dominates.

APPENDIX

Parameterised Ligand-field Calculation.—The discrete $[MNX_4]^-$ ions (M = Os or Ru, X = Cl, Br, or I) possess C_{4v} point symmetry and have metal atoms with a d^2 electronic configuration. If it is assumed that the ligand field is dominated by the axial N^{3-} group then the expected ordering of the metal-based antibonding molecular orbitals would be $d_{xy}^* < d_{x^2-y^2}^* < d_{xz}^*, d_{yz}^* < d_{z^2}^*$. This ordering gives rise to a $(d_{xy}^*)^2$ configuration for the ground state. The excit-

$$\phi_1\ A_1(^1A_1) = \tfrac{1}{2}(|xy^+\,x\bar{y}| - |x\bar{y}\,xy^+|)$$
$$\phi_2\ A_1(^3E) = \frac{i}{2}[|xy^+\,xz^+| - |x\bar{y}\,x\bar{z}| + i(|xy^+\,yz^+| + |x\bar{y}\,y\bar{z}|)]$$
$$\phi_3\ A_2(^3E) = \frac{i}{2}[|xy^+\,xz^+| + |x\bar{y}\,x\bar{z}| + i(|xy^+\,yz^+| - |x\bar{y}\,y\bar{z}|)]$$
$$\phi_4\ B_1(^3E) = \frac{i}{2}[-|xy^+xz^+| + |x\bar{y}\,x\bar{z}| + i(|xy^+yz^+| + |x\bar{y}\,y\bar{z}|)]$$
$$\phi_5\ B_2(^3E) = \frac{i}{2}[|xy^+\,xz^+| + |x\bar{y}\,x\bar{z}| + i(-|xy^+yz^+| + |x\bar{y}\,y\bar{z}|)]$$
$$\phi_6\ E(^3E) = \frac{i}{\sqrt{2}}(|xy^+\,x\bar{z}| + |x\bar{y}\,xz^+|)$$
$$\phi_7\ E(^3E) = \frac{1}{\sqrt{2}}(|xy^+\,yz^-| + |x\bar{y}\,yz^+|)$$
$$\phi_8\ E(^1E) = \frac{i}{\sqrt{2}}(|xy^+\,x\bar{z}| - |x\bar{y}\,xz^+|)$$
$$\phi_9\ E(^1E) = \frac{1}{\sqrt{2}}(|xy^+\,yz^-| - |x\bar{y}\,yz^+|)$$
$$\phi_{10}\ A_1(^3A_2) = \frac{i}{2}(|xy^+\,x^2 - y^2| + |x\bar{y}\,x^2 + y^2|)$$
$$\phi_{11}\ E(^3A_2) = i|xy^+\,x^2 + y^2|$$
$$\phi_{12}\ E(^3A_2) = i|x\bar{y}\,x^2 - y^2|$$
$$\phi_{13}\ A_2(^1A_2) = \frac{i}{\sqrt{2}}(|xy^+\,x^2 + y^2| - |x\bar{y}\,x^2 + y^2|)$$
$$\phi_{14}\ B_1(^3B_2) = \frac{i}{\sqrt{2}}(|xy^+\,z^2| + |x\bar{y}\,z^2|)$$
$$\phi_{15}\ E(^3B_2) = i|xy^+\,z^2|$$
$$\phi_{16}\ E(^3B_2) = i|x\bar{y}\,z^2|$$
$$\phi_{17}\ B_2(^1B_2) = \frac{i}{\sqrt{2}}(|xy^+\,z^2| - |x\bar{y}\,z^2|)$$

$$\begin{array}{l|ccc|} A_1(^1A_1) & H_{11}-E & \xi/2 & \xi/\sqrt{2} \\ A_1(^3E) & \xi/2 & H_{22}-E & -\xi/\sqrt{2} \\ A_1(^3A_2) & \xi/\sqrt{2} & -\xi/\sqrt{2} & H_{1010}-E \end{array} = 0$$

$$\begin{array}{l|cc|} A_2(^3E) & H_{33}-E & -\xi/\sqrt{2} \\ A_2(^1A_2) & -\xi/\sqrt{2} & H_{1313}-E \end{array} = 0$$

$$\begin{array}{l|cc|} B_1(^3E) & H_{44}-E & -\sqrt{3}\xi/\sqrt{2} \\ B_1(^3B_2) & -\sqrt{3}\xi/\sqrt{2} & H_{1414}-E \end{array} = 0$$

$$\begin{array}{l|ccccccccc|} E(^3E) & H_{66}-E & 0 & 0 & \xi/2 & \xi/2\sqrt{2} & -\xi/2\sqrt{2} & -\sqrt{3}\xi/2\sqrt{2} & \sqrt{3}\xi/2\sqrt{2} \\ E(^3E) & 0 & H_{77}-E & \xi/2 & 0 & \xi/2\sqrt{2} & \xi/2\sqrt{2} & \sqrt{3}\xi/2\sqrt{2} & \sqrt{3}\xi/2\sqrt{2} \\ E(^1E) & 0 & \xi/2 & H_{88}-E & 0 & \xi/2\sqrt{2} & \xi/2\sqrt{2} & -\sqrt{3}\xi/2\sqrt{2} & -\sqrt{3}\xi/2\sqrt{2} \\ E(^1E) & \xi/2 & 0 & 0 & H_{99}-E & \xi/2\sqrt{2} & -\xi/2\sqrt{2} & \sqrt{3}\xi/2\sqrt{2} & -\sqrt{3}\xi/2\sqrt{2} \\ E(^3A_2) & \xi/2\sqrt{2} & \xi/2\sqrt{2} & \xi/2\sqrt{2} & \xi/2\sqrt{2} & H_{1111}-E & 0 & 0 & 0 \\ E(^3A_2) & -\xi/2\sqrt{2} & \xi/2\sqrt{2} & \xi/2\sqrt{2} & -\xi/2\sqrt{2} & 0 & H_{1212}-E & 0 & 0 \\ E(^3B_2) & -\sqrt{3}\xi/2\sqrt{2} & \sqrt{3}\xi/2\sqrt{2} & -\sqrt{3}\xi/2\sqrt{2} & \sqrt{3}\xi/2\sqrt{2} & 0 & 0 & H_{1515}-E & 0 \\ E(^3B_2) & \sqrt{3}\xi/2\sqrt{2} & \sqrt{3}\xi/2\sqrt{2} & -\sqrt{3}\xi/2\sqrt{2} & -\sqrt{3}\xi/2\sqrt{2} & 0 & 0 & 0 & H_{1616}-E \end{array} = 0$$

$$\begin{array}{l|cc|} B_2(^3E) & H_{55}-E & \sqrt{3}\xi/\sqrt{2} \\ B_2(^1B_2) & \sqrt{3}\xi/\sqrt{2} & H_{1717}-E \end{array} = 0$$

Where

$$\begin{aligned} H_{11} &= 4F_2 + 36F_4 \\ H_{22} &= -5F_2 - 24F_4 + D_1 + \xi/2 \\ H_{33} &= -5F_2 - 24F_4 + D_1 + \xi/2 \\ H_{44} &= -5F_2 - 24F_4 + D_1 - \xi/2 \\ H_{55} &= -5F_2 - 24F_4 + D_1 - \xi/2 \\ H_{66} &= -5F_2 - 24F_4 + D_1 \\ H_{77} &= -5F_2 - 24F_4 + D_1 \\ H_{88} &= F_2 + 16F_4 + D_1 \\ H_{99} &= F_2 + 16F_4 + D_1 \\ H_{1010} &= 4F_2 - 69F_4 + D_2 \\ H_{1111} &= 4F_2 - 69F_4 + D_2 \\ H_{1212} &= 4F_2 - 69F_4 + D_2 \\ H_{1313} &= 4F_2 + F_4 + D_2 \\ H_{1414} &= -8F_2 - 9F_4 + D_3 \\ H_{1515} &= -8F_2 - 9F_4 + D_3 \\ H_{1616} &= -8F_2 - 9F_4 + D_3 \\ H_{1717} &= 21F_4 + D_3 \end{aligned}$$

$$\begin{aligned} D_1 &= \Delta E(d_{xz}^*, {}_{yz} - d_{xy}^*) \\ D_2 &= \Delta E(d_{x^2-y^2}^* - d_{xy}^*) \\ D_3 &= \Delta E(d_{z^2}^* - d_{xy}^*) \end{aligned}$$

ation of a single electron from the ground state to the above orbitals will give both spin-singlet and spin-triplet excited states of A_2, E, and B_2 symmetry respectively. Based on the assumption that spin–orbit coupling will be a significant perturbation in these systems we have derived the symmetry-determined spin–orbit functions, ϕ, in the C_{4v} point group by using the projection operator.[13]

The energies and functions resulting from the effects of interelectron repulsion, spin–orbit coupling, and d orbital energy separations were calculated by diagonalising the secular determinant. Since there are no off-diagonal terms involving terms of different symmetry this determinant simplifies to the sub-determinants shown.

Crystal-field matrices, including spin–orbit coupling, have been reported by Cowman *et al.*[2] However, our results differ from these in respect of the off-diagonal elements within each sub-determinant. The source of the discrepancy is not known since the wavefunctions used by these authors are not available. In view of this we report our results in some detail.

The wavefunctions resulting from the diagonalisation will be linear combinations of the symmetry-determined spin–orbit functions. We have labelled the final functions according to the origin of the dominant function in the linear combination, *e.g.* $\underline{\psi} = a\psi[A_2(^3E)] + b\psi[A_2(^1A_2)]$, if $a^2 > b^2$ this would be designated $\underline{\psi}[A_2(^3E)]$.

We wish to thank the S.R.C. for financial support.

[1/109 *Received*, 26*th January*, 1981]

REFERENCES

[1] V. Miskowski, H. B. Gray, C. K. Poon, and C. J. Ballhausen, *Mol. Phys.*, 1974, **28**, 747.
[2] C. D. Cowman, W. C. Trogler, K. R. Mann, C. K. Poon, and H. B. Gray, *Inorg. Chem.*, 1976, **15**, 1747.
[3] F. L. Phillips, A. C. Skapski, and M. J. Withers, *Transition Met. Chem.* (*Weinheim*), 1976, **1**, 28.
[4] F. L. Phillips and A. C. Skapski, *J. Cryst. Mol. Struct.*, 1975, **5**, 83; *Acta Crystallogr.*, 1975, **B31**, 2667.
[5] W. P. Griffith and D. Pawson, *J. Chem. Soc., Dalton Trans.*, 1973, 1315.
[6] R. Collin, W. P. Griffith, and D. Pawson, *J. Mol. Struct.*, 1975, **5**, 83.
[7] D. L. McFadden, A. T. McPhail, C. D. Garner, and F. E. Mabbs, *J. Chem. Soc., Dalton Trans.*, 1975, 263.
[8] ' International Tables for *X*-Ray Crystallography,' Kynoch Press, Birmingham, 1962, vol. 3.
[9] J. Lewis and G. Wilkinson, *J. Inorg. Nucl. Chem.*, 1958, **6**, 12.
[10] L. C. Weiss, P. J. McCarthy, J. P. Jasinski, and P. N. Schatz, *Inorg. Chem.*, 1978, **17**, 2689.
[11] M. Gerloch and R. C. Slade, ' Ligand-field Parameters,' Cambridge University Press, 1973, chs. 1 and 9.
[12] D. L. Wood, in Optical Properties of Solids,' eds. S. Nudelman and S. S. Mitra, Plenum Press, New York, 1969, ch. 19.
[13] J. A. Salthouse and M. J. Ware, ' Point Group Character Tables and Related Data, ' Cambridge University Press, 1972, p. 21.